Numerical determination of the profile of the self-similar solution to the 3D Navier-Stokes equations and its applications

Koji Ohkitani
Research Institute for Mathematical Sciences,
Kyoto University, Kyoto 606-8502 Japan

June 2, 2025

Abstract

We present the forward self-similar profile for a particular solution of the 3D Navier-Stokes equations, representing the late stage of decay. The existence of such a profile has been known, but previously its precise functional form has not been determined numerically, let alone mathematically.

In this paper we successfully capture the profile for the first time using numerical methods. This has been achieved by a combination of two things; a numerical method of solving the Navier-Stokes equations in the whole space and the explicit form of the linearised solution. Taking the initial data from the explicit the linearised solution, established in Ohkitani & Vanon (2022), we solve the fully-nonlinear Navier-Stokes equations to observe the convergence to a steady solution in dynamically scaled space. We have confirmed that the deviation from the linearised solution is not large, but appreciable. Some applications of the self-similar profile are discussed briefly.

Navier–Stokes equations, Turbulence theory, Vortex dynamics
MSC Codes 76D05, 35Q30,35C06

1 Introduction

In this paper we study a profile of self-similar solutions as elementary excitations (i.e. building blocks) in viscous incompressible flow.

We review some physical and mathematical models which attempt to introduce elementary excitations. There are a number of attempts to introduce elementary excitations. Literature of physical interest include the following. In Synge & Lin (1943) Hill's spherical vortices were discussed as elementary excitations of 3D turbulent flow. A drawback of this representation is that the skewness factor associated with the model vanishes so that it cannot support non-zero energy transfer. In Chertkov, Pumir, & Shraiman (1999) a phenomenological model based on Lagrangian dynamics of tetrads

was introduced for the 3D Euler equations. This is based on and generalization of Léorat-Vieillefosse-Cantwell model, which ignores the nonlocal term in the expression of the pressure Hessian, Léorat (1975); Vieillefosse (1984); Cantwell (1992). A model of vorticity localised as the Gaussian function such as the Burgers vortex was discussed in Davidson (2015).

On the other hand, mathematical literature include the following works. In Giga & Miyakawa (1989) an extended function class was introduced to accommodate singular initial data for the time evolution of self-similar solutions. The existence of the self-similar profile was proved for small data in Cannone & Planchon (1996). The existence was proved for large data and some estimates were given in Jia & Šverák (2014). They are well summarised in books, e.g. Lemarié-Rieusset (2002, 2018). Most of those works concern proofs of the existence of solutions and the bounds, but estimates are not very much explicit.

It was proved, however, in Jia & Šverák (2014) that the self-similar profile satisfies

$$|U(x) - e^{\triangle} u_0(x)| \leq \frac{C(M)}{(1+|x|)^{1+\alpha}},$$

where $U(x)$ denotes the self-similar profile of velocity, $0 < \alpha < 1$, $C(M)$ a constant and M a norm of the initial data u_0. Note the significance of the symbol $e^{\triangle} = e^{\nu t \triangle}$, where the parameters are takes as $\nu = t = 1$. In Brandolese (2009) an explicit asymptotic formula for far fields was given

$$U(x) = u_0(x) + \triangle u_0(x) - \mathbb{P}\nabla \cdot (u_0 \otimes u_0) - \frac{Q(x) : B}{|x|^7} + O(|x|^{-5} \log |x|),$$

which is valid as $|x| \to \infty$. Here $\mathbb{P}$ denotes solenoidal projection, $u_0(x)$ small initial data, $Q(x)$ a homogeneous cubic polynomial and B a constant matrix. More recent works of related interest include Kukavica & Reis (2011) and Brandolese & Okabe (2024).

It is helpful to recall the two kinds of critical scale invariance; type 1 for which the unknown (vector potential) shares physical dimension with kinematic viscosity ν and type 2, for which the L^1-norm of its n-th spatial derivative shares physical dimension with ν. It should be noted that the heat flow, after dynamic scaling, is not of the Gaussian form. In fact, it is the n-th derivative of the heat flow that takes the Gaussian form.

Our aim here is to define them on the basis of a rational foundation. Before considering the 3D Navier-Stokes equations, we recall the case of the 1D and 2D fluid dynamical equations. For the 1D Burgers equation the velocity profile $U(\xi)$ of the self-similar solution is well-known, e.g. Escobedo & Zuazua (1991)

$$U(\xi) = \frac{C\exp\left(-\frac{a\xi^2}{2\nu}\right)}{1 - \frac{C}{2\nu}\int_0^{\xi} \exp\left(-\frac{a\eta^2}{2\nu}\right) d\eta} \tag{1}$$

$$= -2\nu\partial_{\xi} \log\left(1 - \frac{C}{2\nu}\int_0^{\xi} \exp\left(-\frac{a\eta^2}{2\nu}\right) d\eta\right),$$

the latter of which is reminiscent of the Cole-Hopf transform. Here C denotes a constant, a a zooming-in parameter associated with dynamic scaling, which shares the same physical dimension as kinematic viscosity ν.

On the other hand, for the 2D Navier-Stokes equations vorticity profile $\Omega(\xi)$ of the self-similar solution reads

$$\Omega(\xi) = \frac{a\Gamma}{2\pi\nu} \exp\left(-\frac{a|\xi|^2}{2\nu}\right), \tag{2}$$

where Γ denotes the circulation. Unlike the Burgers equation, the case of the 2D Navier-Stokes equations is degenerate in that no trace of nonlinear terms remains in the self-similar profile. We will see that the case of the 3D Navier-Stokes equations is non-degenerate in that some trace of nonlinear terms does remain in the self-similar profile. We are interested in seeking a counterpart of (1) for the 3D Navier-Stokes equations.

It should be noted that elementary excitations are not identical to the Stokeslets *per se*, which are maintained as a steady solution due to the imposed pressure gradient in the original physical space (that is, before the application of dynamic scaling). Elementary excitations we consider here are steady on their own footing after dynamic scaling.

Motivated by our previous works, we specifically aim to achieve the following objectives.

1) Determination of elementary excitations as defined by a profile of self-similar solutions, which describe the final period of Navier-Stokes flows.

2) Visualisation of the spatial structure of the explicit linearised solutions.

3) Implications on the non-integrability of the Navier-Stokes equations.

Below we begin reviewing some known facts about self-similar solutions of the Navier-Stokes equations and then go through 1) and 2). As for 3), it is generally accepted that the Navier-Stokes equations are not integrable, that is, not exactly reducible to the heat equation. However, no evidence has been given for such an expectation. We give a concrete evidence supporting that this view is indeed the case.

The rest of this paper is constructed as follows. In Section 2 we recall dynamic scaling of the 3D Navier-Stokes equations using different dependent variables. In section 3 we study the linearised self-similar solution in detail. Section 4 is the main results, we report the nonlinear self-similar solution by numerical methods. In section 5 we discuss the non-integrability of the 3D Navier-Stokes equations. Section 6 is devoted to a summary.

2 3D Navier-Stokes equations

We recapitulate the results obtained previously before presenting new results form the numerical experiments.

The 3D Navier-Stokes equations can be written in a number of different ways, using

the vector potential ψ, the velocity u, the vorticity ω and the vorticity curl χ:

$$\frac{\partial \psi}{\partial t} = \frac{3}{4\pi}\text{p.v.}\int_{\mathbb{R}^3} \frac{r \times (\nabla \times \psi(y))\, r \cdot (\nabla \times \psi(y))}{|r|^5}\, \mathrm{d}y + \nu \triangle \psi, \tag{3}$$

$$\frac{\partial u}{\partial t} + u \cdot \nabla u = -\nabla p + \nu \triangle u, \tag{4}$$

$$\frac{\partial \omega}{\partial t} + u \cdot \nabla \omega = \omega \cdot \nabla u + \nu \triangle \omega, \tag{5}$$

$$\frac{\partial \chi}{\partial t} = \triangle(u \cdot \nabla u + \nabla p) + \nu \triangle \chi, \tag{6}$$

where $u = \nabla \times \psi, \omega = \nabla \times u, \chi = \nabla \times \omega, \nabla \cdot \psi = \nabla \cdot u = \nabla \cdot \omega = \nabla \cdot \chi = 0, r = x - y$ and p.v. denotes the principal-value integral.

We consider the dynamically-scaled Navier-Stokes equations for $\Psi(\xi, \tau), U(\xi, \tau), \Omega(\xi, \tau), X(\xi, \tau)$, where

$$\xi = \frac{x}{\sqrt{2at}}, \tau = \frac{1}{2a}\log t,$$
$$\psi = \Psi,\ u = \frac{U}{\lambda(t)},\ \omega = \frac{\Omega}{\lambda(t)^2},\ \chi = \frac{X}{\lambda(t)^3},$$

with $\lambda(t) = \sqrt{2at}$[1] denoting the length scale associated with dynamic scaling. The dynamically-scaled equations read

$$\frac{\partial \Psi}{\partial \tau} = \frac{3}{4\pi}\text{p.v.}\int_{\mathbb{R}^3} \frac{\rho \times (\nabla \times \Psi(\eta))\, \rho \cdot (\nabla \times \Psi(\eta))}{|\rho|^5}\, \mathrm{d}\eta + \nu \triangle \Psi + a(\xi \cdot \nabla)\Psi, \tag{7}$$

$$\frac{\partial U}{\partial \tau} + U \cdot \nabla U = -\nabla P + \nu \triangle U + a(\xi \cdot \nabla)U + aU, \tag{8}$$

$$\frac{\partial \Omega}{\partial \tau} + U \cdot \nabla \Omega = \Omega \cdot \nabla U + \nu \triangle \Omega + a(\xi \cdot \nabla)\Omega + 2a\Omega, \tag{9}$$

$$\frac{\partial X}{\partial \tau} = \triangle\,(U \cdot \nabla U + \nabla P) + \nu \triangle X + a(\xi \cdot \nabla)X + 3aX, \tag{10}$$

where $\nabla \cdot \Psi = \nabla \cdot U = \nabla \cdot \Omega = \nabla \cdot X = 0, \rho = \xi - \eta$. Hereafter, capitalised letters denote those variables defined in the dynamically scaled space. Our aim to solve

$$\triangle\,(U \cdot \nabla U + \nabla P) + \nu \triangle X + a\nabla \cdot (\xi \otimes X) = 0$$

[1] More generally $\lambda(t) = \sqrt{2a(t + t_*)}$, where t_* denotes the virtual time origin. For example, we can take $t_* = 1/(2a)$ to make the dependent variables take identical values before and after scaling.

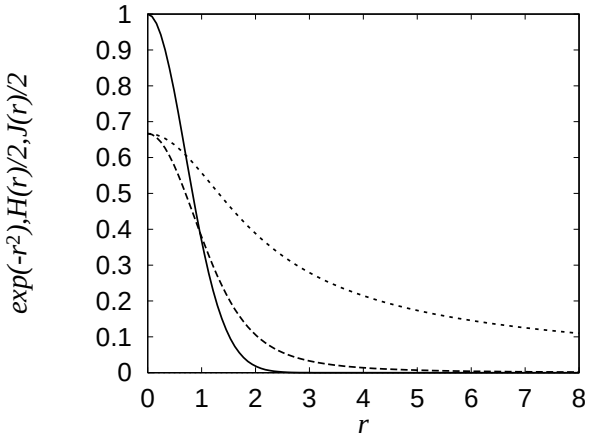

Figure 1: The Gaussian function $\exp(-r^2)$ (solid), $H(r)/2$ (dashed), $J(r)/2$ (dotted).

as accurately and explicitly as possible. We note some basic facts about the problem: (i) It is a steady problem. Hence we can set aside the problem of time evolution on the back burner in the determination of the self-similar profile. (ii) It is a problem of low Reynolds number, but it is still a nonlinear problem.

By Jia & Šverák (2014) we know that $U(\xi)$ exists. By differentiation or integration, we know that $\Psi(\xi), \Omega(\xi)$ and $X(\xi)$ exist as well.

The first order approximation was obtained in Ohkitani & Vanon (2022)

$$\widehat{X} = \mathbb{P}MG, \;\; r = |\xi|, \; \mu = \frac{a}{2\nu}, \; M \equiv \int_{\mathbb{R}^3} X d\xi,$$

where $G(\xi) \equiv \left(\frac{a}{2\pi\nu}\right)^{3/2} \exp\left(-\frac{a}{2\nu}|\xi|^2\right)$ denotes the Gaussian function. It is important to note that when we use vorticity curl X we can easily spot the form of the linerised solutions, because we know that it is the third spatial derivative of Ψ that behaves like a Gaussian function (recall the type 2 scale-invariance). This is not the case when we use more familiar dependent variables, such as velocity or vorticity. Note also that even if the dominant term is taken in vorticity curl, it is *not* purely of the Gaussian form as we see below, because we need to satisfy the incompressible condition.

3 Self-similar solutions of linearised equations

After taking into account the incompressibility condition, the first-order approximation in terms of vorticity curl was given in Ohkitani & Vanon (2022) as follows

$$X_i = M_j \left(\delta_{ij} - \frac{\xi_i\xi_j}{r^2}\right)\left(\frac{\mu}{\pi}\right)^{3/2} e^{-\mu r^2} - M_j \left(\frac{\delta_{ij}}{r^3} - \frac{3\xi_i\xi_j}{r^5}\right)\left\{\frac{\mathrm{erf}(\sqrt{\mu}r)}{4\pi} - \frac{r}{2\mu}\left(\frac{\mu}{\pi}\right)^{3/2} e^{-\mu r^2}\right\}, \tag{11}$$

where summation is implicit for repeated indices.

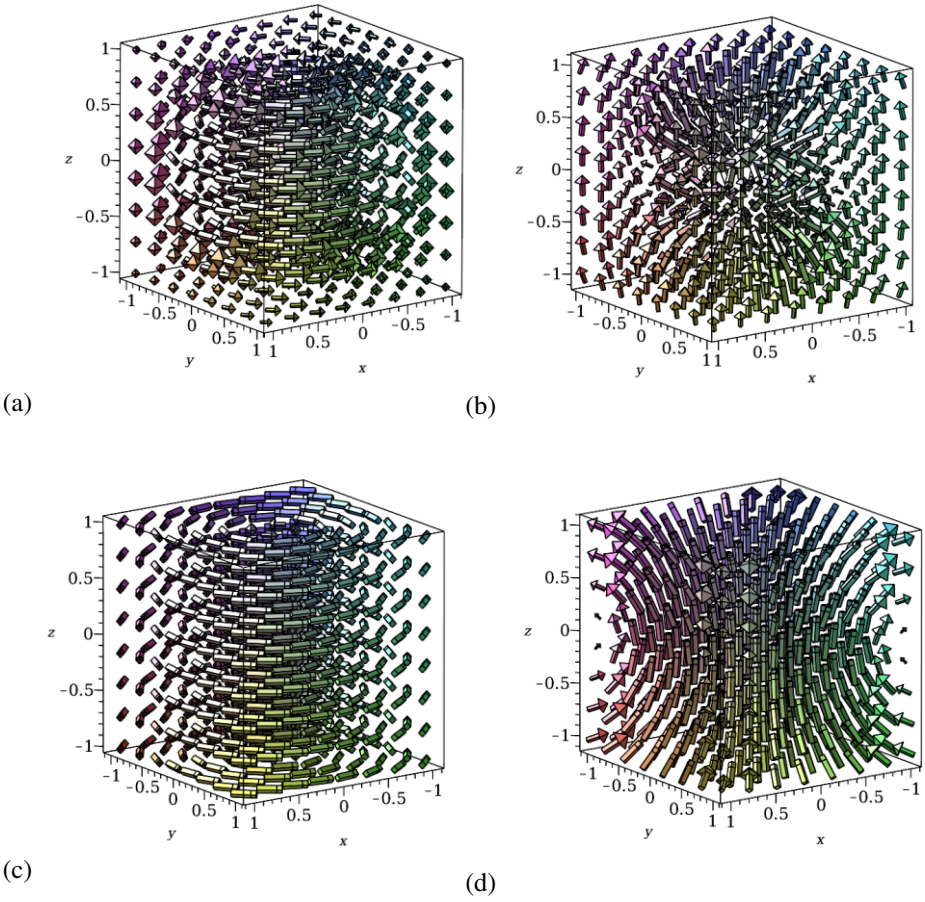

Figure 2: Visualisation of the linearised solution; (a) the vector potential Ψ, (b) the velocity U, (c) the vorticity Ω and (d) the vorticity curl X. The arrow show the directions of Ψ, U, Ω, X, with their length representing the sizes.

We recall the definitions of the two functions introduced for convenience

$$H(r) \equiv \frac{\sqrt{\pi}\mathrm{erf}(r) - 2re^{-r^2}}{r^3},\ J(r) \equiv \frac{re^{-r^2} + \sqrt{\pi}\mathrm{erf}(r)\left(r^2 - \frac{1}{2}\right)}{r^3},$$

both of which are continuous at $r = 0$ (See Figure 1). Note that

$$\lim_{r\to 0} J(r) = \lim_{r\to 0} H(r) = \frac{4}{3},$$

which follows from

$$\mathrm{erf}(r) = \frac{2r}{\sqrt{\pi}}\left(1 - \frac{r^2}{3} + \ldots\right),\ \text{for small } r.$$

Because all the fields are incompressible we also have $U = -\triangle B, \Omega = -\triangle\Psi, X = -\triangle U$. The following expressions in vectorial form were derived in Ohkitani & Vanon (2022);

$$\widehat{\Psi} = \frac{M\times\xi}{8\pi^{3/2}}J(r), \tag{12}$$

$$\widehat{U} = \frac{\mathrm{erf(r)}}{4\pi r}\left(M - \frac{(M\cdot\xi)\xi}{r^2}\right) - \frac{J(r)}{8\pi^{3/2}}\left(M - \frac{3(M\cdot\xi)\xi}{r^2}\right), \tag{13}$$

$$\widehat{\Omega} = \frac{M\times\xi}{4\pi^{3/2}}H(r), \tag{14}$$

$$\widehat{X} = \frac{e^{-r^2}}{\pi^{3/2}}\left(M - \frac{(M\cdot\xi)\xi}{r^2}\right) - \frac{H(r)}{4\pi^{3/2}}\left(M - \frac{3(M\cdot\xi)\xi}{r^2}\right), \tag{15}$$

where $r = |\xi|$.

Taking $M = (1,1,1)$ and $a = 2\nu$ for simplicity, we compare the Gaussian function $e^{-\xi^2}/\pi^{3/2}$ to

$$X_1(\xi,0,0) = \frac{\sqrt{\pi}\mathrm{erf}(\xi) - 2\xi e^{-\xi^2}}{2\pi^{3/2}\xi^3} \quad \left(= \frac{H(\xi)}{2\pi^{3/2}}\right).$$

We observe in Figure 1 that $\pi^{3/2}X_1(\xi,0,0)$ has a longer tail than the Gaussian function $e^{-\xi^2}$.

We show in Figure 2 visualisation of the linearised solution $\widehat{\Psi}, \widehat{U}, \widehat{\Omega}$ and $\widehat{X}$, respectively. It is readily verified that the Frobenius integrability conditions are satisfied;

$$\widehat{\Psi}\cdot\widehat{U} = \widehat{U}\cdot\widehat{\Omega} = \widehat{\Omega}\cdot\widehat{X} = 0.$$

This makes a marked contrast to the property of Beltrami flows, where $\widehat{U}\times\widehat{\Omega} = 0$ holds. They are definitely not Beltrami flows, rather, they have the opposite extreme geometric configuration, where velocity and vorticity perpendicular to each other, rather than parallel.

With use of computer algebra, it can be verified that $X = \mathbb{P}MG$ solves

$$\nu\nabla^2 X + a\nabla\cdot(\xi\otimes X) \equiv \nu\triangle X + a(\xi\cdot\nabla X + 3X) = 0$$

After inverting the gradient operator, we have

$$\nu\nabla X + a\xi \otimes X = \nabla \times f$$

for some $f \neq 0$.

To be explicit, we take for simplicity $\mu = \frac{a}{2\nu} = 1$ and $\xi = (x, y, z)^T$. The x-component of the right-hand side can be found, with use of computer algebra. Unfortunately, it has a complicated form as follows

$$(\nabla \times f)_1 = \left\{(M_2 y + M_3 z)x^4 - M_1(2y^2 + 2z^2 - 3)x^3 + 6(M_2 y + M_3 z)x^2\right.$$

$$\left. -2M_1\left(y^2 + z^2 + \frac{9}{4}\right)(y^2 + z^2)x - (y^2 + z^2)\left(y^2 + z^2 + \frac{3}{2}\right)(M_2 y + M_3 z)\right\}\frac{e^{-r^2}}{r^3}$$

$$+\left\{M_1 x^5 + \frac{3}{2}(M_2 y + M_3 z)\,x^4 + \frac{M_1}{2}(y^2 + z^2 - 3)x^3 + \frac{3}{2}(y^2 + z^2 - 2)(M_2 y + M_3 z)x^2\right.$$

$$\left. -\frac{M_1}{2}(y^2 + z^2)\left(y^2 + z^2 - \frac{9}{2}\right)x + \frac{3}{4}(y^2 + z^2)(M_2 y + M_3 z)\right\}\frac{\sqrt{\pi}\mathrm{erf}(r)}{r^{7/2}},$$

where other components can be obtained by cyclic permutations.

4 Self-similar solutions of nonlinear equations

4.1 Numerical methods

In Ohkitani & Vanon (2022) we introduced an iteration scheme which yielded the leading order approximation. However, it seems difficult to extend this approach to higher orders and obtain the nonlinear solution. We also attempted to simulate dynamically scaled Navier-Stokes equations directly for a long time in order to achieve the convergence to a steady solution. However, this did not work either, because of the badly behaved $x \cdot \nabla$ term at far distances. Furthermore, an attempt to apply the method of integrating factors has been made, but to no avail.

That is why we have decided to solve the Navier-Stokes equations numerically in the original physical space and dynamically-scale the solutions to see whether its profile converges to a steady solution in the transformed space. Actually, this simplistic approach does work and we will describe the results below.

To simulate flows on $\mathbb{R}^3$ we use the simple method of domain truncation, that is, instead of $\mathbb{R}^3$, we consider a cube $[-L, L]^3$ of size $2L$, which is large in comparison with the characteristic length scale of the flow field in question. Numerically, this box has a set of grid points $\{(x_j, y_k, z_l); j, k, l = -N, \ldots, N\}$, where $x_j = y_j = z_j = Lj/N$, $j = -N, \ldots, N$, for some positive integer N.

Firstly, we solve the Navier-Stokes equations in the form of the vorticity equations, using a central finite difference scheme for them. The numerical scheme is similar to the one used in studying the 2D Navier-Stokes equations in $\mathbb{R}^2$, Ohkitani, K. (2023) and its details to be described elsewhere, Ohkitani, K. (2025). We use a fast Poisson solver

for handling the Biot-Savart relationship to recover the velocity from the vorticity. The zero Dirichlet boundary conditions are imposed

$$\omega(x, y, \pm L) = \omega(\pm L, y, z) = \omega(x, \pm L, , z) = 0, \ -L \le x, y, z \le L,$$

where the vorticity can be regarded as small at the box boundaries. This approach seems plausible and has been checked *a posteori*, that is, confirming the smallness of the vorticity field near the boundaries.

We use the following numerical parameters: $L = 20$, $N = 128$ (corresponding to 257^3 collocation points). For time marching the fourth order Runge-Kutta scheme was used. All the computations were done in the double precision arithmetic.

For the initial condition we use the linearised solution $\omega(x, 0) = \widehat{\Omega}(x)$, defined in (3.4), which is known to be close to the fully nonlinear solution. After obtaining $\omega(x, t)$ on the time interval $0 \le t \le 100$ by numerical methods with a time step $\Delta t = 5 \times 10^{-3}$, we dynamically-scale it as

$$\Omega(\xi, \tau) = (1 + 4\nu t)\, \omega(x, t),$$

where $\xi = \frac{x}{\sqrt{1+4\nu t}}$, $\tau = \frac{1}{4\nu} \log(1 + 4\nu t)$.

Secondly, we solve the 3D Navier-Stokes equations in velocity form, again using a central finite difference scheme. We use a fast Poisson solver for handling the Biot-Savart relationship for estimating the pressure. Here, the Dirichlet boundary conditions are imposed at the edges of the box as

$$u(x, y, \pm L) = u(\pm L, y, z) = u(x, \pm L, , z) = 0, \ -L \le x, y, z \le L,$$

where the velocity can be regarded as small at the box boundaries. It is clear that this condition is harder to satisfy because, generally speaking, the velocity field decays more slowly than the vorticity does. Time marching is done by the fourth-order Runge-Kutta method on the time interval $0 \le t \le 100$, with $\Delta t = 5 \times 10^{-3}$. We take $L = 20$ and $N = 100$ which corresponds to the number of collocation points 201^3. We have checked that the numerical solutions are unaffected when we change the parameters by doubling them like $L = 40$ and/or $N = 200$.

For the initial condition we use the linearised solution $u(x, 0) = \widehat{U}(x)$, defined in (3.3), which is known to be close to the nonlinear solution. After obtaining $u(x, t)$ numerically, we dynamically-scale the dependent variable, this time, as follows

$$U(\xi, \tau) = \sqrt{1 + 4\nu t}\, u(x, t).$$

Finally, to check the CFL condition we estimate $u_{\max} \frac{\Delta t}{\Delta x} = 6 \times 10^{-3} \frac{5 \times 10^{-3}}{0.2} = 1.5 \times 10^{-4} \ll 1$ at $t = 0$. At later times that is even smaller, which implies stability of the time marching scheme.

4.2 Numerical results

We present the results obtained by solving the vorticity equations, using the following physical parameters $\nu = 2 \times 10^{-2}$, $\mu = a/(2\nu) = 1$. We first check the validity of the

Navier-Stokes solver in the whole space $\mathbb{R}^3$ by cutting off the nonlinear terms. In Figure 3 we show thus obtained solution after scaling transformations. A perfect agreement of the profiles is observed, consistent with the steadiness in the dynamically-scaled space. No matter how trivial this may seem, it gives an important check. This is because it firstly confirms the analytical representation of the linearised solution (3.4), and secondly justifies the numerical methods employed herein. It confirms particularly that the vorticity decays quickly to zero in the region $|\xi| \leq 5$. Note that the computational domain is $|\xi| \leq L/\sqrt{1+4\nu t} = \sqrt{20}/3 \approx 6.6$ at $t = 100$. At the boundaries the vorticity $\omega(x)$ is typically on the order of $O(10^{-4})$, or $\Omega(\xi)$ is on the order of $O(10^{-3})$ at $t = 100$.

Now we reinstate the nonlinear terms and solve fully nonlinear equations. In Figure 4 we show the nonlinear solution in the transformed space. We observe that the profile does evolve in time, but it converges to a fixed form quickly. This confirms that our numerical method captures the nonlinear solution successfully and the steady state represents the profile we are after. In Figure 5 we show time evolution of the enstrophy

$$Q(t) = \frac{1}{2}\int_{\mathbb{R}^3} |\omega|^2 dx$$

for both linearised and linear solutions. Essentially both linear and nonlinear curves collapse, (actually, independent of the formalism in vorticity or velocity). It shows the enstrophy decays to about 25% of its initial value during the time interval $0 \leq t \leq 100$. Now that the the evolution of enstrophy is virtually indistinguishable between the linearised and nonlinear solutions, one possible interpretation of the deviation is a slight spatial translation in vorticity.

To double-check that a solution converges in dynamically-scaled space we next solve the Navier-Stoke equations in velocity form. Again we have confirmed that the linearised solution remains unchanged in dynamically-scaled space (figure omitted). To test the convergence of $U(\xi, \tau)$ in Figure 6 we plot $U_1(\xi, \xi, \xi)$ at several different times. We confirm the profile converges to a fixed form, which means the numerical method captures the self-similarity profile in velocity as well. As noted above, the zero Dirichlet boundary conditions are harder to meet, the velocity $u(x)$ at the boundaries is typically on the order of $O(7 \times 10^{-4})$, or, $U(\xi)$ on the order of $O(10^{-3})$, say, at $t = 100$.

Nonetheless, the enstrophy $Q(t)$ calculated from the thus-obtained velocity field is indistinguishable from Figure 5, both for linearised and nonlinear solutions. This indicates that the computations are robust in spite of the boundary conditions, which are hard to satisfy with velocity.

To estimate the deviation of the nonlinear steady solution from the linearised solution

$$\Delta U_1 = U_1(\xi, \xi, \xi) - \widehat{U}_1(\xi, \xi, \xi),$$

we plot $\Delta U_1(\xi, \xi, \xi)$ in Figure 7 at $t = 100$. The size of the deviation is not large, but appreciable. The leading-order asymptotic analysis of the self-similar profile given in Ohkitani & Vanon (2022), shows the normalised deviation (in X) is of $O(10^{-2})$, as opposed to the $O(10^{-1})$ deviation (in U) for the Burgers equation. This means that the cumulative effects of higher order terms in the successive approximation give rise to an appreciable deviation.

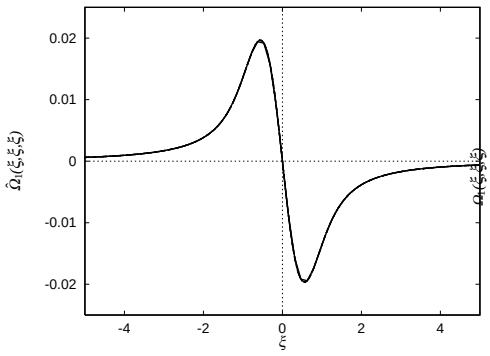

Figure 3: A sectional plot of the vorticity field $\widehat{\Omega_1}(\xi,\xi,\xi)$ (linearised solution), at $t = 0$(solid), 20(dashed), 40(dotted), 60(dash-dotted), 80(thick-solid), 100(dash triple-dotted). All six curves collapse.

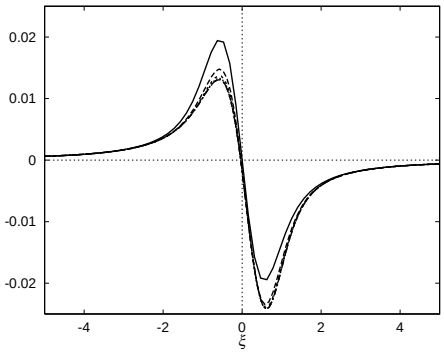

Figure 4: A sectional plot of the vorticity field $\Omega_1(\xi,\xi,\xi)$ (nonlinear solution), at $t = 0$(solid), 20(dashed), 40(dotted), 60(dash-dotted), 80(thick-solid), 100(dash triple-dotted).

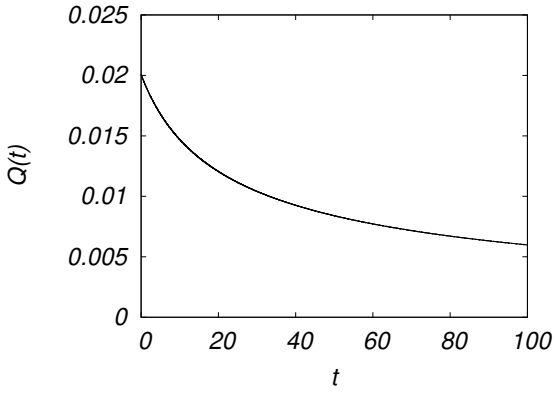

Figure 5: Time evolution of the enstrophy, from vorticity form: nonlinear (solid), linear (dashed) and from velocity form: nonlinear (dotted), linear (dash-dotted). All the four curves basically collapse.

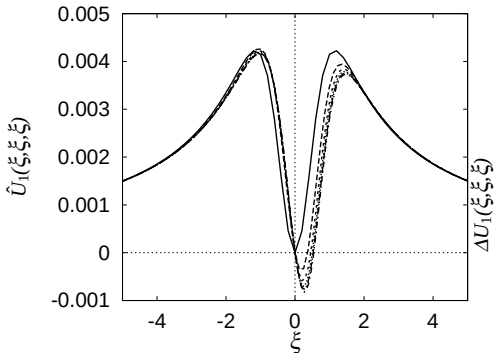

Figure 6: Convergence to the self-similar profile in velocity at $t = 0$(solid), 20(dashed), 40(dotted), 60(dash-dotted), 80(thick-solid), 100(dash triple-dotted).

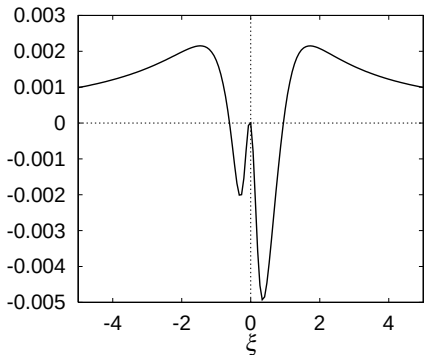

Figure 7: Subdominant term in the self-similar profile at $t = 100$.

5 Non-integrability of the Navier-Stokes equations

We begin considering the following question; *Can* $\Psi(\xi), U(\xi), \Omega(\xi)$ *and* $X(\xi)$ *be expressed as a function of* $\widehat{\Psi}(\xi), \widehat{U}(\xi), \widehat{\Omega}(\xi)$ *and* $\widehat{X}(\xi)$*, respectively ?* A short answer is 'yes' for $U(\xi)$ and $X(\xi)$, but 'no' for $\Psi(\xi)$ or $\Omega(\xi)$. We will give more detailed explanations below.

Invertibility of hatted (that is, linearised) variables in scaled space means that for $\widehat{\Psi} = \widehat{\Psi}(\xi)$ we can find some function F such that $\xi = F(\widehat{\Psi})$ holds, under some conditions, that is,

$$\text{If } \frac{\partial(\widehat{\Psi_1}, \widehat{\Psi_2}, \widehat{\Psi_3})}{\partial(\xi_1, \xi_2, \xi_3)} \neq 0, \text{then } \begin{cases} \xi_1 =^{\exists} f_1(\widehat{\Psi}), \\ \xi_2 =^{\exists} f_2(\widehat{\Psi}), \\ \xi_3 =^{\exists} f_3(\widehat{\Psi}). \end{cases}$$

When this is the case, in principle we can plug them into $\Psi = \Psi(\xi)$ and write $\Psi(\xi) =^{\exists} F(\widehat{\Psi})$ for some function F. In fact, it has turned out with computer algebra that

$$\det\left(\frac{\partial\widehat{\Psi}}{\partial\xi}\right) = \frac{\partial(\widehat{\Psi}_1, \widehat{\Psi}_2, \widehat{\Psi}_3)}{\partial(\xi_1, \xi_2, \xi_3)} \equiv 0,$$

$$\det\left(\frac{\partial\widehat{\Omega}}{\partial\xi}\right) = \frac{\partial(\widehat{\Omega}_1, \widehat{\Omega}_2, \widehat{\Omega}_3)}{\partial(\xi_1, \xi_2, \xi_3)} \equiv 0.$$

Hence, even though Ψ and $\widehat{\Psi}$ are close to each other, it is not guaranteed that the former can be represented by a function of the latter.[2] The same goes for Ω and $\widehat{\Omega}$.

[2] It *would* be a real surprise if $\det\left(\frac{\partial\widehat{\Psi}}{\partial\xi}\right) \neq 0$, almost everywhere.

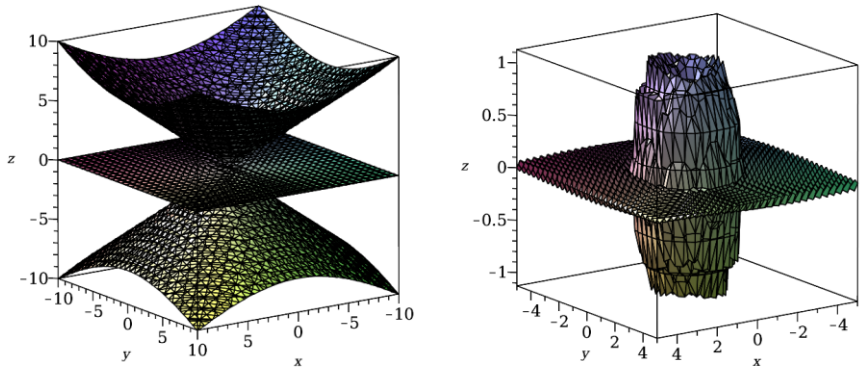

(a) (b)

Figure 8: Visualisation of surfaces of zeros of Jacobian determinants: (a) the velocity U and (b) the vorticity curl X. Here $(x, y, z) = (\xi_1, \xi_2, \xi_3)$.

On the other hand, in contrast we have found

$$\det\left(\frac{\partial \widehat{U}}{\partial \xi}\right) = \frac{\partial(\widehat{U}_1, \widehat{U}_2, \widehat{U}_3)}{\partial(\xi_1, \xi_2, \xi_3)} \neq 0,$$

$$\det\left(\frac{\partial \widehat{X}}{\partial \xi}\right) = \frac{\partial(\widehat{X}_1, \widehat{X}_2, \widehat{X}_3)}{\partial(\xi_1, \xi_2, \xi_3)} \neq 0.$$

Hence $\widehat{U}$ and U are related by some mapping and so are $\widehat{X}$ and X. We can write in principle

$$U = F_1(\widehat{U}), \;\; X = F_2(\widehat{X}),$$

for some functions F_1, F_2.

More specifically, we find with computer algebra

$$\det\left(\frac{\partial U}{\partial \xi}\right) = -\frac{z}{128\pi^{9/2}(s^2+z^2)^{15/2}}$$

$$\times\left\{\pi(s^2+z^2-\frac{3}{2})\left(s^6+(2z^2-\frac{9}{4})s^4+(z^4+\frac{9}{4}z^2-\frac{27}{8})s^2+\frac{9}{4}z^4-\frac{27}{8}z^2\right)\right.$$

$$\times\sqrt{s^2+z^2}(\operatorname{erf}\sqrt{s^2+z^2})^2 e^{-(s^2+z^2)}$$

$$+6\sqrt{\pi}(s^2+z^2)\left(s^6+(2z^2-\frac{9}{8})s^4+(z^4+\frac{9}{8}z^2-\frac{27}{16})s^2+\frac{9}{8}z^4-\frac{27}{4}z^2\right)$$

$$\left.\times\operatorname{erf}\sqrt{s^2+z^2}e^{-2(s^2+z^2)}\right.$$

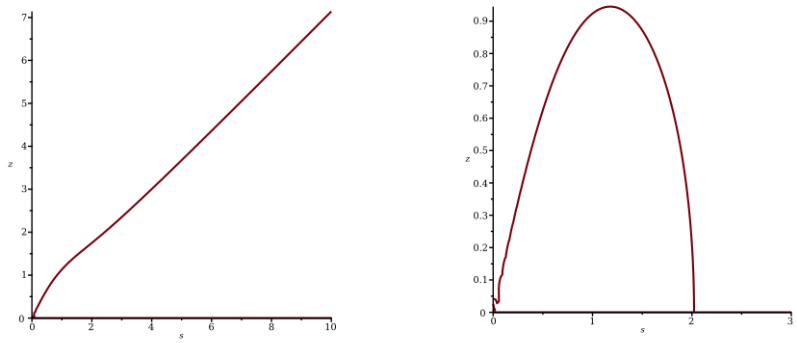

Figure 9: Sectional plots of zeros of (a) the Jacobian of $\widehat{U}$ and (b) that of $\widehat{X}$, plotted z- vs. r-axes.

$$+9\left(s^4+(z^2+\frac{3}{4})s^2+\frac{3}{2}z^2\right)(s^2+z^2)^{3/2}e^{-3(s^2+z^2)}$$

$$-\frac{1}{4}(s^2+z^2-\frac{3}{2})^2\left(s^4+(-z^2+\frac{3}{2})s^2-2z^4+3z^2\right)\pi^{3/2}(\mathrm{erf}\sqrt{s^2+z^2})^3\Big\},$$

and

$$\det\left(\frac{\partial X}{\partial\xi}\right)=\frac{2z}{\pi^{9/2}(s^2+z^2)^{15/2}}$$

$$\times\Bigg[\frac{1}{16}(s^2+z^2)^{3/2}\left(z^4(4s^2+4)+(8s^4+6s^2+6)z^2+4s^6+2s^4+3s^2\right)(2s^2+2sz^2+3)^2e^{-3(s^2+z^2)}$$

$$-\frac{3\sqrt{\pi}}{2}(s^2+z^2)\mathrm{erf}\sqrt{s^2+z^2}\left(z^4(s^2+\frac{3}{2})+(2s^4+\frac{9}{4}s^2+\frac{9}{4})z^2+s^6+\frac{3}{4}s^4+\frac{9}{8}s^2\right)(s^2+z^2+\frac{3}{2})e^{-2(s^2+z^2)}$$

$$+\frac{9\pi}{16}\sqrt{s^2+z^2}(\mathrm{erf}\sqrt{s^2+z^2})^2\left(z^4(s^2+3)+(2s^4+\frac{9}{2}s^2+\frac{9}{2})z^2+s^6+\frac{3s^4}{2}+\frac{9s^2}{4}\right)e^{-(s^2+z^2)}$$

$$-\frac{27}{128}\pi^{3/2}(\mathrm{erf}\sqrt{s^2+z^2})^3(s^2+2z^2)\Bigg],$$

where

$$s^2\equiv x^2+y^2.$$

For U and X, the Jacobian determinants vanish on surfaces (i.e. sets of measure zero) as in Figure 8. We also show their sectional plots in Figure 9. Invertibility is assured almost everywhere, except for those surfaces. By the inverse function theorem the self-similar profile in velocity (resp. vorticity curl) can be represented as a function of their linearised counterparts. It should be noted that it is $\Psi(\xi)$ which corresponds to the heat flow in the dynamically-scaled space. Recall that it is the error function which corresponds to the heat flow in the source-type solution of the 1D Burgers equation (1).

These are non-trivial results, but not very useful with regard to the problem of integrability. It doesn't tell us how a Navier-Stokes solution can be constructed from a heat flow, because neither $\widehat{U}$ nor $\widehat{X}$ represents the heat flow in dynamically scaled space.

6 Applications

One application is a particular solution to the Hopf equation the late-stage of decay. Consider the Hopf functional for the vorticity curl

$$\Phi[\theta(\xi),t]=\left\langle \exp\left(i\int_{\mathbb{R}^3}\chi(x,t)\cdot\theta(\xi)dx\right)\right\rangle,$$

where the brackets denote an ensemble average. Given $\Phi[\theta(\xi),\tau]$, by reverting to the original variables

$$\chi(x,t)=\frac{1}{\{2a(t+t_*)\}^{3/2}}X(\xi,\tau),\ \xi=\frac{x}{\sqrt{2a(t+t_*)}},\ \tau=\frac{1}{2a}\log\frac{t+t_*}{t_*},$$

we have

$$\Phi=\Phi\left[\theta\left(\frac{x}{\sqrt{2a(t+t_*)}}\right),\frac{1}{2a}\log\frac{t+t_*}{t_*}\right],$$

which defines a particular self-similar solution to the Hopf equation, Ohkitani & Vanon (2022).

For the 3D Navier-Stokes equations the existence of self-similar solutions is known (in velocity) in a number of function spaces. The corresponding vorticity gradient gives the source-type solution implicitly. With this variable it is near-Gaussian and we have the vorticity curl in its scaled form $X(\xi)\sim\exp\left(-\frac{a}{2\nu}|\xi|^2\right)$, where the effects of nonlinear terms and incompressibility should be taken into account.

We can in principle write

$$X(\xi)=F\left[\exp\left(-\frac{a}{2\nu}|\xi|^2\right);M\right],$$

where F denotes a *near-identity* non-local functional and $M=\int_{\mathbb{R}^3}X(\xi)d\xi$ an invariant. With this understanding the late-stage Hopf functional can be written

$$\Phi[\theta(\xi)]=\int\exp\left(i\int_{\mathbb{R}^3}F\left[\exp\left(-\frac{a}{2\nu}|\xi|^2\right);M\right]\cdot\theta(\xi)d\xi\right)d\mu(M),$$

where an ensemble mean is to be taken over different values of M. In the linearised approximation recall that we have

$$X(\xi)\equiv F\left[\exp\left(-\frac{a}{2\nu}|\xi|^2\right);M\right]\approx\mathbb{P}MG\equiv\widehat{X}(\xi)$$

Note that $X(0)$ is a constant vector, as a function of M, but we do not know its functional form yet. We confirm that the above form is a generalisation of the Hopf-Titt solution of the Hopf functional equation, Hopf & Titt (1953). Indeed, in their linearised approximation we have

$$\Phi[\theta(\xi)]\approx\int\exp\left(i\int_{\mathbb{R}^3}\mathbb{P}MG\cdot\theta(\xi)d\xi\right)d\mu(M).$$

Let $X_0(\xi) = \mathbb{P}M\delta(\cdot)$, then the exponent reads

$$i\int_{\mathbb{R}^3}(G*X_0)(\xi)\cdot\theta(\xi)d\xi = i\int_{\mathbb{R}^3}X_0(\xi)\cdot(G*\theta)(\xi)d\xi$$

$$= i\exp\left(\frac{\nu}{2a}D\right)\int_{\mathbb{R}^3}X_0(\xi)\cdot\theta(\xi)d\xi,$$

where the symbol $\exp(t\nu D)$ represents the time development operator over an interval $[0,t]$ of $\theta(x)$ by the heat kernel.

Hence

$$\Phi[\theta(\xi)] \approx \exp\left(\frac{\nu}{2a}D\right)\Phi_0[\theta(\xi)],$$

or

$$\Phi[\theta(x)] \approx \exp\left(\nu t D\right)\Phi_0[\theta(x)]$$

in the original variables, which is nothing but the Hopf-Titt solution, Hopf & Titt (1953).

Finally, it is in order to make a brief comment on a possible model of a 'point' singularity for 3D Euler flows. In the limit of $a/\nu \to \infty$ in (2), we have formally $\Omega(\xi) \to \delta(\xi)$, where $\delta(\dot{})$ denotes the Dirac mass. This is the point vortex known for 2D Euler flows. We will consider whether its 3D counterpart is available or not.

Consider two kinds of singular distributions; the vorticity localised along a curve (line vortex) and the vorticity curl localised at a point (like a Dirac mass) associated with algebraically decaying terms for maintaining the incompressibility. They are dual in that they share the strength of singularity in Sobolev norm $H^{1/2}$, or equivalently, the form of energy spectrum $E(k) \propto k^{-2}$.

Taking the limit of $\mu \to \infty$ in (11), we find formally

$$X \to \frac{2}{3}M\delta - \frac{1}{4\pi}\left(\frac{M}{r^3} - \frac{3(M\cdot\xi)\xi}{r^5}\right), \tag{16}$$

under the assumption that $\frac{\xi_i\xi_j}{r^2}\delta \to (\delta_{ij}/3)\delta$ as $r \to 0$. It is of interest to observe that the same expression is obtained when we compute, under the assumption that $\lim_{\mu\to\infty}\mathbb{P}MG = \mathbb{P}M\lim_{\mu\to\infty}G$,

$$\chi = \mathbb{P}M\delta = (I - \triangle^{-1}\nabla\nabla\cdot)M\delta$$

$$= \frac{2}{3}\kappa\delta - \frac{1}{4\pi}\left(\frac{\kappa(t)}{r^3} - \frac{3(\kappa\cdot x)x}{r^5}\right),$$

where, for simplicity, we now write x for the spatial coordinates and denote $r = |x|$. In passing, we note that in other dependent variables the model takes the following forms

$$\omega = \frac{1}{4\pi}\frac{\kappa\times x}{r^3},\quad u = \frac{1}{8\pi}\left(\frac{\kappa}{r} + \frac{(\kappa\cdot x)x}{r^3}\right),\quad \psi = \frac{1}{8\pi}\frac{\kappa\times x}{r},$$

and that, in particular, the following relationship holds $\psi = \frac{r^2}{2}\omega$.

That being said, the limit passage is actually inconsistent in that the volume integrals of both sides of (16) do not match, when carried over a large sphere centered at the

singular point. The mismatch, i.e. the left-hand side = M whereas the right-hand side = $\frac{2}{3}M$, due to the local diagonal term $\delta(x)/3$ associated with the singular integrals,

$$\frac{\partial^2}{\partial x_i \partial x_j}\frac{1}{4\pi|x|} = -\frac{\delta_{ij}}{3}\delta(x) - \mathrm{p.v.}\frac{1}{4\pi}\left(\frac{\delta_{ij}}{|x|^3} - \frac{3x_i x_j}{|x|^5}\right).$$

We hence refrain from pursuing the idea further here.

7 Summary

In this paper we have studied self-similar solutions to the Navier-Stokes equations, centering on the following topics. (1) Numerical determination of the elementary excitations (as self-similar solutions). (2) Characterisation of the spatial structure via visualisation of linerised solutions. (3) Non-integrability of the Navier-Stokes equations, where presence or otherwise of functions mapping linearised solutions to nonlinear ones is studied.

We have reported on the successful capture of the nonlinear profile of self-similar solution to the Navier-Stokes equations. It is of interest to seek an analytical expression of the profile approximately, because this has been achieved by numerical methods. That would be useful for asymptotic analysis of the decaying process of the Navier-Stokes flows. This is left for future study.

[Acknowledgements]This work was supported by the Research Institute for Mathematical Sciences, an International Joint Usage/Research Center located in Kyoto University.

[Funding]This work was also supported by JSPS KAKENHI Grant Number JP22K03434.

[Declaration of interests]The author reports no conflict of interest.

[Data availability statement]The data that support the findings of this study are openly available in [repository name] at http://doi.org/[doi], reference number [reference number]. See JFM's research transparency policy for more information

[Author ORCIDs]K. Ohkitani, https://orcid.org/0000-0001-7261-9724

[Author contributions]Authors may include details of the contributions made by each author to the manuscript'

A Different forms of linearised solutions

We can alternatively write

$$\widehat{U} = \frac{1}{8\pi^{3/2}}\left(2J(r)M + \xi \times (M \times \xi)\frac{J'(r)}{r}\right),$$

$$\widehat{X} = \frac{1}{4\pi^{3/2}}\left(2H(r)M + \xi \times (M \times \xi)\frac{H'(r)}{r}\right),$$

where

$$J'(r) = \frac{2\sqrt{\pi}\mathrm{erf}(r) - 3rJ(r)}{r^2}, \quad H'(r) = \frac{4e^{-r^2} - 3H(r)}{r}.$$

Note $(M \times \xi) \cdot U = (M \times \xi) \cdot X = 0$.

Yet another equivalent expression is as follows

$$\widehat{U} = \left(\frac{\mathrm{erf}(r)}{8\pi r} + \frac{H(r)}{16\pi^{3/2}} \right) M + \left(\frac{\mathrm{erf}(r)}{8\pi r} - \frac{3H(r)}{16\pi^{3/2}} \right) \frac{(M \cdot \xi)\xi}{r^2}.$$

This is convenient for numerical computations.

References

Brandolese, L. 2009 Fine properties of self-similar solutions of the Navier–Stokes equations, *Arch. Rat. Mech. Anal.*, **192**, 375–401.

Brandolese, L. & Okabe, T. 2024 Forced rapidly dissipative Navier–Stokes flows, *SIAM J. Math. Anal.*, **56**, 412-432.

Cannone, M. and Planchon, F. 1996 Self-similar solutions for Navier-Stokes equations in $\mathbb{R}^3$, *Commun. in P.D.E.*, **21**, 179–193.

Cantwell, B.J. 1992 Exact solution of a restricted Euler equation for the velocity gradient tensor *Phys. Fluids A*, **4**, 782–793.

Chertkov, M., Pumir, A., & Shraiman, B.I. 1999 Lagrangian tetrad dynamics and the phenomenology of turbulence, *Phys. fluids*, **11**, 2394–2410.

Davidson, P. 2015 Turbulence: an introduction for scientists and engineers, Oxford University Press.

Escobedo, M. & Zuazua, E. 1991 Large time behavior for convection-diffusion equations in R^N, *J. Func. Anal.*, **100**, 119–161.

Foias, C. and Saut, J.-C. 1982 Transformation fonctionnelle linéarisant les equation de Navier-Stokes, *C. R. Acad. Sc. Paris, Série I*, **285**, 325–327 .

Fujigaki, Y. and Miyakawa, T. 2001 Asymptotic profiles of nonstationary incompressible Navier–Stokes flows in the whole space, *SIAM J. Math. Anal.*, **33**, 523–544.

Giga, Y. and Miyakawa, T. 1989 Navier-Stokes flow in R^3 with measures as initial vorticity and Morrey spaces, *Commun. Partial Diff. Eqns.*, **14**, 577–618.

Hopf, E. & Titt, E.W. 1953 On certain special solutions of the Φ-equation of statistical hydrodynamics, *J. Rat. Mech. Anal.*, **2**, 587–591.

Jia H. & Šverák V. 2014 Local-in-space estimates near initial time for weak solutions of the Navier-Stokes equations and forward self-similar solutions, *Invent. Math.*, **196**, 233–265.

Kukavica, I. and Reis, E. 2011 Asymptotic expansion for solutions of the Navier–Stokes equations with potential forces, *J. Diff. Equations*, **250**, 607–622.

Lemarié-Rieusset, P.G. 2002 *Recent developments in the Navier-Stokes problem*, CRC Press.

Lemarié-Rieusset, P.G. 2018 *The Navier-Stokes problem in the 21st century*, Chapman and Hall/CRC.

Léorat, J. 1975 La turbulence megnetohydrodynamique helicitaire et la generation des champs magnetique a grande echelle, Thèse de Doctorat, L'Université de Pari -VII.

Ohkitani, K. & Vanon, R. 2022 Self-similar source-type solutions to the three-dimensional Navier–Stokes equations, *Proc. R. Soc. A.*, **478**, 20210527.

Ohkitani, K. 2022 Self-similarity in turbulence and its applications, *Phil. Trans. R. Soc. A*, **380**, 20210048.

Ohkitani, K. 2023 Numerical comparison of two-dimensional Navier-Stokes flows on the whole plane and the periodic domain, *Phys. Rev. Fluids*, **8**, 124607.

Ohkitani, K. 2025 Numerical comparison of three-dimensional Navier-Stokes flows on the whole space and the periodic domain, in preparation.

Saffman, P.G. 1997 Vortex models of isotropic turbulence, *Phil. Trans. Roy. Soc. Lond, Ser. A*, **355**, 1949–1956.

Synge, J.L. & Lin, C.C. 1943 On a statistical model of isotropic turbulence, *Trans. R. Soc. Canada*, **37**, 45–79.

Vieillefosse, P. 1984 Internal motion of a small element of a fluid in inviscid flow, *Physica A*, **125**, 150–162.